The Astrophysical Journal, 961:93 (11pp), 2024 January 20 https://doi.org/10.3847/1538-4357/ad0cea

The Sloan Digital Sky Survey Reverberation Mapping Project: Investigation of Continuum Lag Dependence on Broad-line Contamination and Quasar Properties

Hugh W. Sharp[1], Y. Homayouni[2,3], Jonathan R. Trump[1], Scott F. Anderson[4], Roberto J. Assef[5], W. N. Brandt[2,3,6], Megan C. Davis[1], Logan B. Fries[1], Catherine J. Grier[7], Patrick B. Hall[8], Keith Horne[9], Anton M. Koekemoer[10], Mary Loli Martínez-Aldama[11], David M. Menezes[1], Theodore Pena[7], C. Ricci[5,12], Donald P. Schneider[2,3], Yue Shen[13,14], and Benny Trakhtenbrot[15]

[1] Department of Physics, 196 Auditorium Road, Unit 3046, University of Connecticut, Storrs, CT 06269 USA; hugh.sharp@uconn.edu
[2] Department of Astronomy & Astrophysics, 525 Davey Lab, The Pennsylvania State University, University Park, PA 16802, USA
[3] Institute for Gravitation and the Cosmos, The Pennsylvania State University, University Park, PA 16802, USA
[4] Astronomy Department, University of Washington, Box 351580, Seattle, WA 98195, USA
[5] Instituto de Estudios Astrofísicos, Facultad de Ingeniería y Ciencias, Universidad Diego Portales, Avenida Ejército Libertador 441, Santiago, Chile
[6] Department of Physics, 104 Davey Lab, The Pennsylvania State University, University Park, PA 16802, USA
[7] Department of Astronomy, University of Wisconsin-Madison, Madison, WI 53706, USA
[8] Department of Physics and Astronomy, York University, 4700 Keele Street, Toronto, ON M3J 1P3, Canada
[9] SUPA Physics and Astronomy, University of St. Andrews, St. Andrews, Fife KY16 9SS, Scotland, UK
[10] Space Telescope Science Institute, 3700 San Martin Drive, Baltimore, MD 21218, USA
[11] Astronomy Department, Universidad de Concepción, Barrio Universitario S/N, Concepción 4030000, Chile
[12] Kavli Institute for Astronomy and Astrophysics, Peking University, Beijing 100871, People's Republic of China
[13] Department of Astronomy, University of Illinois at Urbana-Champaign, Urbana, IL 61801, USA
[14] National Center for Supercomputing Applications, University of Illinois at Urbana-Champaign, Urbana, IL 61801, USA
[15] School of Physics and Astronomy, Tel Aviv University, Tel Aviv 69978, Israel
Received 2023 September 1; revised 2023 November 1; accepted 2023 November 14; published 2024 January 17

Abstract

This work studies the relationship between accretion-disk size and quasar properties, using a sample of 95 quasars from the Sloan Digital Sky Survey Reverberation Mapping Project with measured lags between the g and i photometric bands. Our sample includes disk lags that are both longer and shorter than predicted by the Shakura and Sunyaev model, requiring explanations that satisfy both cases. Although our quasars each have one lag measurement, we explore the wavelength-dependent effects of diffuse broad-line region (BLR) contamination through our sample's broad redshift range, $0.1 < z < 1.2$. We do not find significant evidence of variable diffuse Fe II and Balmer nebular emission in the rms spectra, nor from Anderson–Darling tests of quasars in redshift ranges with and without diffuse nebular emission falling in the observed-frame filters. Contrary to previous work, we do not detect a significant correlation between the measured continuum and BLR lags in our luminous quasar sample, similarly suggesting that our continuum lags are not dominated by diffuse nebular emission. Similar to other studies, we find that quasars with larger-than-expected continuum lags have lower 3000 Å luminosities, and we additionally find longer continuum lags with lower X-ray luminosities and black hole masses. Our lack of evidence for diffuse BLR contribution to the lags indicates that the anticorrelation between continuum lag and luminosity is not likely to be due to the Baldwin effect. Instead, these anticorrelations favor models in which the continuum lag increases in lower-luminosity active galactic nuclei, including scenarios featuring magnetic coupling between the accretion disk and X-ray corona, and/or ripples or rims in the disk.

Unified Astronomy Thesaurus concepts: Quasars (1319); Active galactic nuclei (16); Supermassive black holes (1663)

1. Introduction

Active galactic nuclei (AGNs) are the most luminous persistent sources of radiation in our Universe, and are characterized by nonstellar spectra that are driven by an accreting disk of matter falling toward a supermassive black hole (SMBH; Lynden-Bell 1969). Observations demonstrate that all massive galaxies have a central SMBH (e.g., Magorrian et al. 1998; Kormendy & Ho 2013), indicating that AGNs, as rapidly growing SMBHs, are important to the field of galaxy evolution as a whole (Di Matteo et al. 2003; Hopkins et al. 2005a, 2005b; Di Matteo et al. 2005). The majority of SMBH growth is governed by rapid accretion (e.g., Soltan 1982), so understanding the detailed geometry and emission profile of these disks is critically important for SMBH buildup and its connection to galaxy evolution.

In general, the physical components that comprise the innermost regions of AGNs are not spatially resolvable (for exceptions, see Gravity Collaboration et al. 2018; Event Horizon Telescope Collaboration et al. 2019; Markoff & Event Horizon Telescope Collaboration 2022). Thus, measurement of AGN scale and structure most commonly relies on reverberation mapping (RM; e.g., Blandford & McKee 1982; Peterson et al. 2004; Cackett et al. 2021), a method utilizing time-domain monitoring to substitute temporal resolution for spatial resolution. The method relies on the characteristic variability of a quasar's central emission being reemitted ("reverberated") by more distant material, delayed (or "lagged") by the light-crossing time ($\tau = R/c$) of the system (Cackett et al.

2007, 2021). The natural temperature gradient of the system causes the peak emission of hotter, more central regions, to occur at shorter wavelengths, while regions at larger radii have peak emission at longer wavelengths (e.g., Collier et al. 1998; Sergeev et al. 2005; McHardy et al. 2014; Shappee et al. 2014). By measuring the time delays between variability features in light curves observed in various wavelengths, we can recover information on the scale and structure of various AGN components, characterized by the relative locations of their observed emission. The RM method was first implemented to measure the size of the broad-line region (BLR), but can be used to measure other parts of the AGN's inner environment, including the X-ray corona, accretion disk, and dusty torus (Cackett et al. 2021, and references therein). In particular, the accretion-disk structure is probed by utilizing continuum RM, where the lag between variability features is measured between multiple UV and optical continuum light curves, driven by (unobserved) central X-ray ionization (Cackett et al. 2007).

For an idealized geometrically thin, optically thick, steady-state accretion disk, the Shakura & Sunyaev (1973; SS73) model describes the relationship between disk size, black hole mass, accretion rate, and emission wavelength:

$$\tau \propto (M_{\rm BH}\dot{M})^{1/3}\lambda^{4/3}, \quad (1)$$

where $\tau = R/c$ is the observed lag, $\lambda \propto 1/T$ for blackbody peak emission, and T is the temperature of the disk. For accretion-disk lag measurements in large continuum-RM surveys, the above equation is often fit by the function $\tau = \tau_0[(\lambda/\lambda_0)^{\beta} - 1]$, where τ_0 is a normalization factor, λ_0 is a reference wavelength, and β represents the wavelength exponent in Equation (1). In the case of local, single-object studies (McHardy et al. 2014; Edelson et al. 2015, 2017; Fausnaugh et al. 2016; McHardy et al. 2018), the wavelength dependence of the disk lag appears to agree with that of the SS73 model (Equation (1)), where $\beta \sim 4/3$. The normalization factor indicative of scale, τ_0, on the other hand, has generally been reported to be ∼2–3 times larger than anticipated.

UV/optical observations of continuum RM require a high temporal resolution (∼1 day) due to the small relative distance between wavelength regions. This requirement has limited the application of large surveys to study accretion-disk size over a large sample until very recently. Large surveys like Pan-STARRS (Jiang et al. 2017), the Dark Energy Survey (Mudd et al. 2018; Yu et al. 2020), and the Sloan Digital Sky Survey (SDSS; Homayouni et al. 2019) have found that $\beta \sim 4/3$; thus, the wavelength dependence of the lag is in agreement with Equation (1). The normalization factor τ_0, conversely has had differing results from the SS73 prediction among these surveys. Of these larger studies mentioned, Jiang et al. (2017) and Mudd et al. (2018) find τ_0 to be ∼2–3 times larger than anticipated, similar to single-object studies. Yu et al. (2020) and Homayouni et al. (2019) argue the average disk lag of their surveys agree with the SS73 model, but with large scatter in individual disk lags that significantly exceeds the observational uncertainties. Homayouni et al. (2019) also discuss that the larger lags reported by other surveys may be due to biases toward large lags in cadence-limited observations.

In addition, a few accretion-disk scales have been observed via gravitational microlensing of quasars, a different process entirely from continuum RM. In cases such as Morgan et al. (2010), the optical emitting region representing the disk is larger than expected, similar to the general findings of continuum RM. These measurements could however suffer from observational biases due to a combination of the inclination of the disk relative to the line of sight and the differential magnification of the temperature fluctuations, producing overestimated disk sizes (Tie & Kochanek 2018).

These larger-than-anticipated disk sizes have many possible explanations. The SS73 model may simply be overidealized; for example, it does not properly describe basic features of quasars such as variability (Dexter & Agol 2010). Many studies include different disk structures and/or radiative-transfer effects that produce larger disk sizes than predicted by the SS73 model. Dexter & Agol (2010) suggest that local fluctuations in the accretion disk produce a larger overall disk size. Following this interpretation, Neustadt & Kochanek (2022) constructed and tested a new model to describe AGN continuum variability based on ingoing and outgoing axisymmetric temperature fluctuations waves. Their results yielded similar "blue-leading-red" variability as the contemporary "lamppost" model most RM studies ascribe to, while characterizing a more slowly varying component observed in some quasar light curves. Separately, Hall et al. (2018) show that with a sufficiently low accretion-disk atmospheric density, scattering in the atmosphere can produce a nonblackbody emergent spectrum, also resulting in larger disk lags. Additionally, Mummery & Balbus (2020) suggest that larger disk lags can occur in disks dominated by tidal disruption events. Starkey et al. (2023) also demonstrated that invoking a disk geometry with a steep rim or rippled structures will result in increased irradiated luminosity, and thus temperature, producing reverberation lags that are larger than the simple SS73 thin disk picture. Gaskell (2017) suggest the internal reddening of AGNs is more significant than ordinarily considered, leading to underestimated bolometric luminosity. As such, the SS73 expectation which is proportional to $L^{1/3}$ would also be underestimated, explaining the comparatively larger measured accretion-disk lag.

Different emission reprocessing models have also been shown to produce larger continuum lags. Kammoun et al. (2019) and Kammoun et al. (2021) study disk-reprocessing models with general relativistic ray tracing and find that a larger X-ray corona height tends to yield systematically larger lags. Sun et al. (2020) introduce the corona-heated accretion-disk-reprocessing (CHAR) model, in which the corona and the accretion disk are coupled via a magnetic field. Energy transfer by magnetic heating adds an additional time delay for disk reprocessing that is related to the thermal timescale ($\tau_{\rm TH}$) in addition to the light-crossing time, increasing the lags for lower-mass black holes in particular. In addition, there is potential for nebular continuum emission to affect the measured disk lag. As discussed by Cackett et al. (2018), photometric observations can be contaminated by diffuse emission from the BLR, resulting in an increased lag localized to these diffuse-emitting regions. Chelouche et al. (2019) and Cackett et al. (2022) argue that all UV/optical photometric filters may be contaminated by substantial diffuse continuum emission from the boundary of the outer accretion disk and BLR.

To understand better the cause behind these larger disk sizes, we study the detailed quasar properties for the 95 objects with measured disk lags from Homayouni et al. (2019). While the average lag of this sample was found to be consistent with the

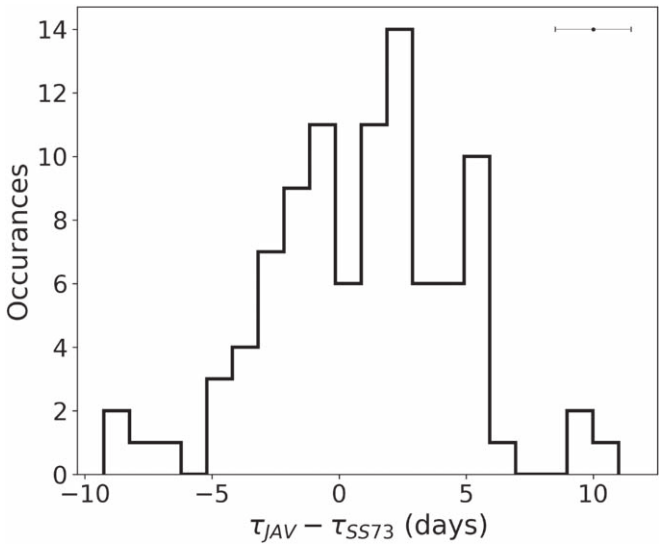

Figure 1. The distribution of the offset between the observed disk lags obtained using JAVELIN, and the disk lag anticipated by the SS73 model using Equations (2) and (3). Only 36% of the sample fall within 1σ of the SS73 prediction, and additionally have an excess scatter of $\sigma\tau/\tau = 1.35$, implying there is an intrinsic scatter in disk size within this quasar sample.

SS73 model, the lags have a much broader distribution than expected given the measurement uncertainties, with an excess scatter of $\sigma\tau/\tau = 1.35$ (see Figure 1). These quasars were monitored as a part of the SDSS-RM Project (Shen et al. 2015), utilizing both broad-line RM (Grier et al. 2017) to obtain black hole mass ($M_{\rm BH}$) measurements, and continuum RM in the g and i bands to measure accretion-disk scale and structure (Homayouni et al. 2019). In addition, these 95 SDSS targets cover a large range of quasar properties, such as black hole mass, luminosity (L), and Eddington ratio ($\lambda_{\rm Edd} = L/L_{\rm Edd}$), each spanning ~3 magnitudes, among others provided by Shen et al. (2019), over the redshift range of $0.1 < z < 1.2$. Studying these disk lags and their deviation from the SS73 model among such a broad quasar demographic can expose systematic trends and reveal necessary accretion physics missing from the model.

In Section 2, we discuss the sample of 95 quasars used in Homayouni et al. (2019), including observations, measurement of disk lags, and construction of rms residual spectra. In Section 3 we discuss the patterns and correlations (or the lack thereof) that arise when comparing the observed continuum lags to various quasar properties. We conclude in Section 4 with a discussion of the implications of our observations for models of accretion-disk structure and emission reprocessing.

2. Data

This study includes 95 SDSS-RM quasars with continuum lags measured by Homayouni et al. (2019) in order to understand better how accretion-disk structure depends on quasar properties. The SDSS-RM project (Shen et al. 2015) monitored a total of 849 quasars in a 7 deg^2 field. The sample spans a broad range of redshifts, black hole masses, luminosities, and other quasar properties (Shen et al. 2019), making it a useful sample for studying the diversity of quasar accretion-disk structure. A subset (44) of the black hole masses are measured from broad-line RM by Grier et al. (2017), while the remainder are estimated from single-epoch scaling relations (as described in Shen et al. 2019; Dalla Bontà et al. 2020). We additionally use X-ray luminosities from XMM-Newton imaging of the field (Liu et al. 2020).

2.1. Observations and Light Curves

We use continuum lags and rms spectra measured from the first year (2014) of SDSS-RM observations. This includes 32 epochs of spectroscopic monitoring from the SDSS/BOSS instrument (Dawson et al. 2013), from which synthetic g and i photometry were extracted using the SDSS filter response functions (Fukugita et al. 1996). The light curves include an additional 63 epochs of photometric monitoring from the Bok 2.3 m and Canada–France–Hawaii Telescope (CFHT) 3.6 m telescopes (Kinemuchi et al. 2020). Observations from the three observatories (SDSS, Bok, and CFHT) were intercalibrated and combined using the CREAM software (Starkey et al. 2015).

2.2. Disk Lag Measurements

Homayouni et al. (2019) measure the lags between observed-frame g- and i-band light curves through two methods: an interpolated cross-correlation function (ICCF; Gaskell & Sparke 1986; Gaskell & Peterson 1987; White & Peterson 1994; Peterson et al. 2004) and JAVELIN (Zu et al. 2011). ICCF uses simple linear interpolation to reconstruct the light curve during monitoring gaps in the observations, and calculates the Pearson coefficient r between them across a range of allowed τ, thus producing a cross-correlation function. JAVELIN more robustly accounts for monitoring gaps by fitting the bluest light curve with a damped random walk (DRW) model. Observations have shown that a DRW model is appropriate in describing the variability of a quasar light curve on timescales relevant for RM studies (Kelly et al. 2009; Kozłowski et al. 2010; MacLeod et al. 2010). JAVELIN uses the constructed DRW model of the blue light curve and performs a parameterized fit to the responding light curve, assuming that the responding light curve is a shifted, smoothed, and scaled version of the model, thus recovering τ.

Each of these methods use Monte Carlo techniques to estimate the lag uncertainty, which are discussed in further detail in Homayouni et al. (2019). Lag estimates from both methods were found to be consistent in our sample, whereas the lag uncertainties produced from ICCF seem to be overestimated in comparison to those produced by JAVELIN. This is consistent with the results of Yu et al. (2020), which demonstrate that the JAVELIN uncertainties are more accurate and the ICCF uncertainties are overestimated for light curves with the characteristics of those from SDSS-RM. We thus use the JAVELIN lags and uncertainties of the 95 SDSS-RM quasars to explore their diversity in accretion-disk size. These lags are considered "well defined" among a larger sample of 222 targets, passing three selective criteria presented in Homayouni et al. (2019) to ensure the lags were not subject to measurement bias. These criteria filtered out targets that exhibited a low cross-correlation coefficient to eliminate uncorrelated light curves, ambiguous lag detection resulting from bimodal probability distributions, and significant broad-line contribution from C IV, Mg II, Hβ, and Hα emission lines, with specific quantitative thresholds defined in Homayouni et al. (2019).

2.3. Spectroscopic Data and PrepSpec

All these targets have spectra collected throughout the duration of SDSS-RM observations, each with 90 epochs from 2014 to 2020. We use these data to probe quasar properties associated with emission lines. PrepSpec, described in Shen et al. (2016), was used to create both time-averaged and rms spectra in the optical/UV, giving the average and variability amplitude of the spectra over those 90 epochs. PrepSpec decomposes time-resolved spectra into a model considering wavelength- and time-dependent components for the continuum and broad and narrow emission lines, creating a model of the mean quasar spectra. PrepSpec also creates model rms spectra that are a measure of variability of the modeled components over our 90 epochs observed for each of our quasars. As will be discussed further in Section 3.2, we utilize the modeled rms spectra to investigate variability of the diffuse nebular continuum as a potential bias in the lag measurements of our quasars.

3. Results

3.1. Comparing τ_{jav} to τ_{SS73}

We compare the measured lags from Homayouni et al. (2019) with the lags predicted by the SS73 model. Observing in the g and i bands, the disk lag predicted by the SS73 model is as follows:

$$\tau_{\rm SS73} = \frac{\tau_0}{(1+z)^{1/3}}\left[\left(\frac{\lambda_i}{\lambda_0}\right)^{4/3} - \left(\frac{\lambda_g}{\lambda_0}\right)^{4/3}\right]. \quad (2)$$

Here Homayouni et al. (2019) use a normalized wavelength of $\lambda_0 = \lambda/9000$ Å and produce a disk normalization, τ_0, representative of a realistic disk size. The analytic form of τ_0 is given as:

$$\tau_0 = \frac{1}{c}\left(\frac{45G}{16\pi^6 h_p c^2}\right)^{1/3} X^{4/3}(\lambda_0)^{4/3}\left(\frac{C_{\rm Bol}}{\eta c^2}\right)^{1/3} M_{\rm BH}^{1/3}\lambda L_{\lambda 3000}^{1/3}. \quad (3)$$

Here $C_{\rm Bol} = 5.15$ is the bolometric luminosity correction (Richards et al. 2006) and $\eta = 0.1$ was chosen as the radiative efficiency. The factor X accounts for the wavelength range of blackbody emission at a given temperature, originating from any given accretion-disk radius, where $X = \frac{hc}{\lambda k T(\lambda)}$. We adopt the value $X = 2.49$ which Fausnaugh et al. (2016) derive from a flux-weighted mean radius.

As noted by Homayouni et al. (2019), the average disk lag of the sample is consistent with $\tau_{\rm SS73}$, but with a large scatter. This scatter is greater than the observational uncertainties, with only 36% of the sample of 95 quasars falling within 1σ of the model lags as highlighted in Figure 1. As JAVELIN has been thoroughly tested to produce accurate uncertainties (Yu et al. 2020), the broad distribution of measured lags indicates genuine excess scatter compared to the SS73 model expectation. We adopted two variables to quantify the observed SS73 model deviations, the disk lag offset ($\tau_{\rm jav} - \tau_{\rm SS73}$) and disk lag ratio ($\tau_{\rm jav}/\tau_{\rm SS73}$), when testing for correlations with quasar properties.

3.2. Diffuse Contamination

When comparing the disk lag offsets to redshifts as seen in Figure 2, by visual inspection, our quasars seem to exhibit a larger scatter in disk lag offset toward higher z, specifically around the range $0.8 < z < 1.0$ (henceforth referred to as $z_{\rm con}$). This redshift range is notable because it corresponds to the regime in which our photometry may be contaminated by diffuse Fe II emission in the g band and diffuse Balmer emission in the i band. Diffuse emission from gas in the more distant BLR can cause longer than anticipated lags contributing to the observed i-band emission, as well as shorter lags if present in the g band (Netzer 2022). Evidence for longer lags due to diffuse Balmer emission has been found previously in single-target, intensive campaigns with a multiband lag analysis (Edelson et al. 2019; Hernández Santisteban et al. 2020; Vincentelli et al. 2022). For example, Cackett et al. (2018) create a "lag spectrum" that comprises the measured disk lag as a function of wavelength for NGC 4593, finding a broad excess in the measured lag leading up to the Balmer jump (3640 Å). Chelouche et al. (2019), Cackett et al. (2022), and Netzer (2022) present further evidence that diffuse BLR emission may additionally affect multiple photometric bands in addition to the strong effect from the Balmer continuum.

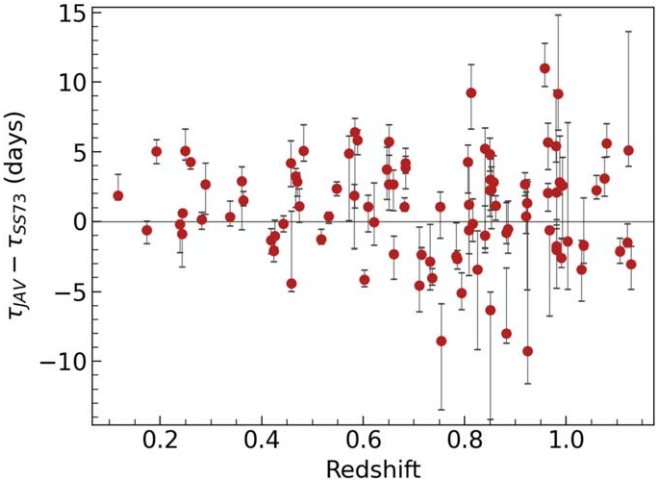

Figure 2. The sample of 95 quasars with their disk lag offset ($\tau_{\rm jav} - \tau_{\rm SS73}$) plotted vs. redshift. The sample's disk lag offsets noticeably increase in scatter within $0.8 < z < 1.0$. At this redshift range, the g and i photometric bands reside in regions of diffuse Balmer and Fe II emission, respectively, which may be contributing to the variability in our light curves.

We performed a statistical analysis to determine whether the distribution of disk lags is significantly different between the populations of quasars inside and outside $z_{\rm con}$. Figure 3 splits the disk lag distribution given in Figure 1 into these regions in redshift. If there is no redshift dependence on disk lag offset, both of these particular quasar distributions should be drawn from a similar parent distribution of disk lag offset. We used a k-sample Anderson–Darling (AD) test to determine whether the distribution of disk lag offsets inside and outside $z_{\rm con}$ can be statistically drawn from the same parent population. The k-sample AD tests the null hypothesis that k samples are drawn from the same population without having to specify the distribution function of the parent population, as detailed in Scholz & Stephens (1987). Using the scipy.stats (Virtanen et al. 2020) implementation of the k-sample AD test, we find p-value > 0.05. This indicates that we cannot confidently reject that the disk lag offset distributions of these two quasar samples differ from the parent distribution when separated in redshift based on potential contamination. As the AD test is inconclusive, we next study the variable spectra of

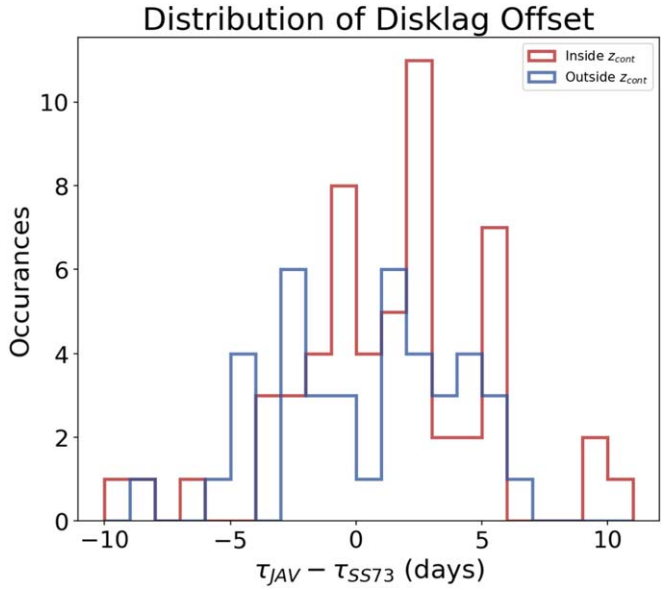

Figure 3. Disk lag offset distribution shown in Figure 1 split into a distribution of targets within z_{con} (in red) and outside z_{con} (in blue). Our k-sample AD test was unable to reject the null hypothesis that these distributions are drawn from the same population.

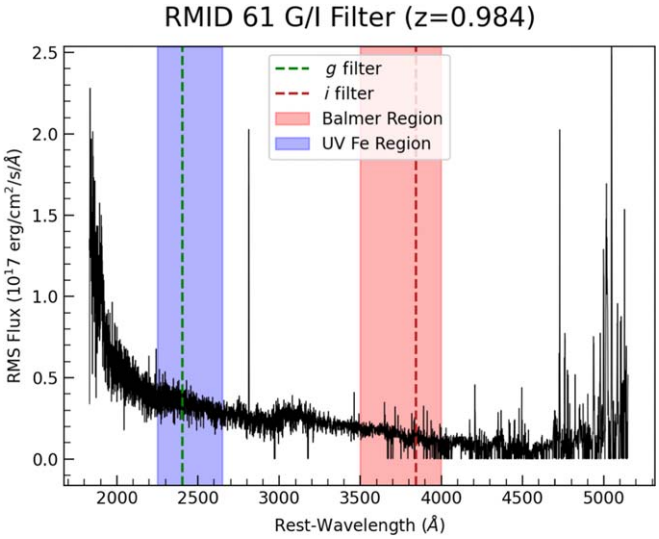

Figure 4. An example rms spectrum of RMID 61, a quasar within z_{con} at $z = 0.98$. The blue and red shaded regions represent the wavelength ranges of diffuse Fe II and Balmer emission, respectively, while the dashed green and red lines represent the central wavelengths of the g and i photometric filters for this quasar, respectively. As shown here, there is possible contamination in RMID 61 in both the g and i bands as they fall within the regions of diffuse UV Fe and Balmer emission, respectively.

our quasars to search for direct evidence for such contamination as demonstrated in Figure 4.

We also quantified the variability of the diffuse Balmer and Fe II emission by measuring their equivalent widths (EWs) from the rms spectra. Quasars with significantly variable diffuse BLR emission that biases the measured g–i lag should have a larger contribution to their rms spectra. Thus measuring these EWs in the rms spectra should indicate whether these diffuse emission features have substantial variability in comparison to the continuum. We made EW measurements in rest-frame wavelength ranges 3500–4000 and 2250–2650 Å to probe for diffuse Balmer and Fe II, respectively. To ensure complete coverage of the wavelength range for nebular continuum emission (and reliable continuum estimates around the diffuse emission), we restricted the diffuse Balmer sample to $z > 0.3$ and the diffuse Fe II sample to $z > 0.6$, measuring EWs for 84 and 55 quasars, respectively, out of our sample's total of 95. The rms continuum fit by `PrepSpec` was normalized to the rms flux around 3000 Å in the rest frame to avoid prominent emission lines. Figure 5 presents two examples of rms spectra that have significant diffuse continuum emission. We estimate the EW uncertainties using a Monte Carlo method, adding random Gaussian noise associated with the uncertainties of the rms spectra for each pixel in wavelength.

Figure 6 reveals our quasar sample spans a large range of diffuse Fe II and Balmer EW measurements in the rest frame. When fitting via `linmix`'s implementation of linear regression (Kelly 2007), no correlation was detected between either the diffuse Fe II and Balmer rms EWs and the disk lag offsets of our sample. Even at the extrema of $\tau_{\rm jav} - \tau_{\rm SS73}$, these quasars do not appear to have the significantly larger diffuse Balmer EWs for the longer lags and larger diffuse Fe II EWs for shorter lags that we would expect if diffuse BLR emission contributes to their lag measurements. Even a visual inspection suggests few of these quasar spectra have diffuse features apparent in the rms spectra as shown in Figure 5, and those displayed do not have particularly extreme deviations from their predicted SS73 result. This behavior is similar NGC 4593 covered in Cackett et al. (2018), where the excess lag in the 3000–4000 Å regime implies diffuse Balmer contamination, but there does not appear to be any significant increase in the rms spectra of NGC 4593 in the 3000–4000 Å range.

Lastly, Wang et al. (2023) propose that if continuum lag measurements are dominated by diffuse BLR emission, there should be a tight correlation between continuum and BLR lags. Continuum lags dominated by diffuse BLR emission would further imply an $R_{\rm cont}$–L relation that is analogous to the $R_{\rm BLR}$–L correlation, notably used to estimate the bulk of black hole mass growth over cosmic time (e.g., Vestergaard & Osmer 2009). A relationship between continuum lags and luminosity would be far less observationally demanding than the time-domain spectroscopy required for BLR lag measurements. Wang et al. (2023) report a correlation between $R_{\rm BLR}$ and R_{5100}, which they further use to imply an R_{5100}–L relation, where R_{5100} is the continuum size at rest-frame 5100 Å. To investigate a similar correlation in the SDSS-RM sample, we use the subset of 30 quasars that both feature well-measured disk sizes from Homayouni et al. (2019) and reliable Hβ BLR size measurements from Grier et al. (2017). We then convert the observed-frame g–i lag to the rest-frame time delay between the inner accretion disk to the rest-frame 5100 Å emission region [$\tau_{5100} = \tau_0(\lambda_0 = 5100$ Å)]. Similar to Wang et al. (2023), we assume a wavelength dependence of $\beta = 4/3$ and convert the g–i lag measurements as shown below, following a similar form of Equation (2):

$$\tau_{5100} = \tau_{\rm jav}(1+z)^{1/3}\left[\left(\frac{\lambda_i}{5100\text{Å}}\right)^{4/3} - \left(\frac{\lambda_g}{5100\text{Å}}\right)^{4/3}\right]^{-1}. \quad (4)$$

Figure 7 presents a comparison of the SDSS-RM targets with the result from Wang et al. (2023). To accommodate for the upper limits of some of the continuum lag measurements as censored data, we flip the axes between the τ_{5100} and Hβ BLR

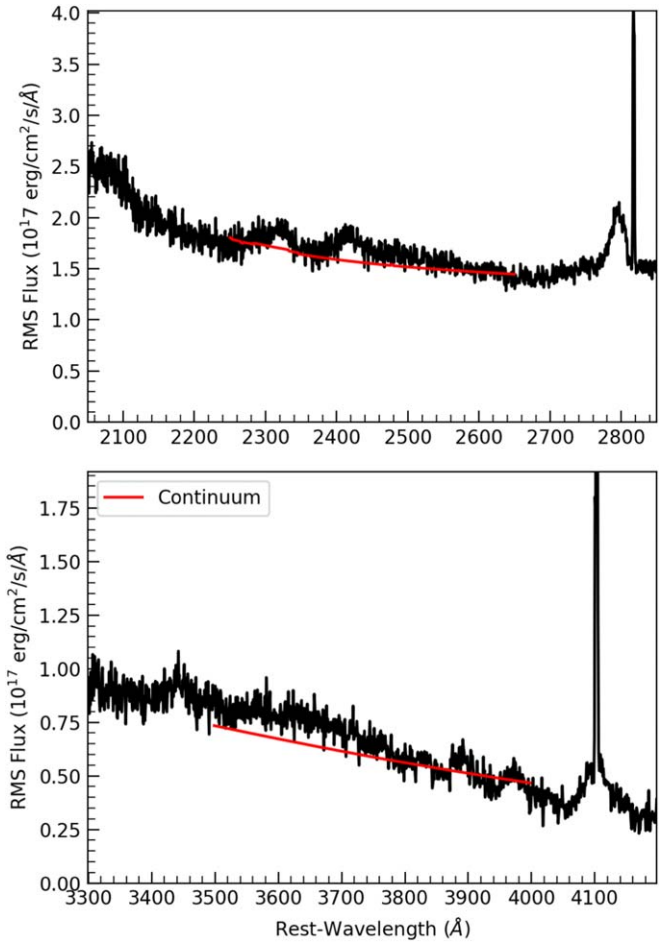

Figure 5. Examples of targets containing noticeable diffuse contamination in their rms spectrum (black) as identified from a continuum fit (red lines). In the top plot, RMID 428 has excess variable emission in the 2250–2650 Å region consistent with diffuse Fe UV emission. In the bottom plot, RMID 160 has excess variable emission compared to the continuum over ∼3500–3700 Å, which is consistent with diffuse Balmer emission.

sizes compared to Wang et al. (2023) and convert their best-fit line to the case where τ_{5100} is regressed to $\tau_{\rm BLR}$. Among the 30 SDSS-RM quasars with reliable disk size measurements and Hβ BLR measurements, we identify seven quasars with negative continuum lag measurements. We perform a survival analysis using the software package `PyStan`, treating the seven negative lags as censored data, and we then perform a linear regression, which produces a slope of $0.25^{+0.21}_{-0.23}$ (consistent with no correlation) with $\sigma = 0.26$ intrinsic scatter. Figure 7 displays the result of our survival analysis and the best-fit line to the total of 30 SDSS-RM quasars. We find no correlation between continuum lag and Hβ lag among the luminous quasars of the SDSS-RM sample, consistent with our previous conclusions that the continuum lags of these quasars are not dominated by diffuse BLR emission.

3.3. Disk Size and Quasar Properties

To understand better the deviations in the observed disk lags versus those predicted by the SS73 model, we broadly searched for correlations between various quasar properties and logarithmic disk lag ratio ($\log(\tau_{\rm jav}/\tau_{\rm SS73})$). We also tested for correlations between our quasar properties and disk lag offset ($\tau_{\rm jav} - \tau_{\rm SS73}$), as would be appropriate for linearly scaled quasar properties. Our tested quasar properties include optical and X-ray luminosities, black hole mass, Eddington ratio, and various spectral properties associated with "eigenvector 1" (Boroson & Green 1992; Sulentic et al. 2001; Shen & Ho 2014), and ionization hardness as inferred from the narrow-line L[O III]/L(Hβ) ratio. We fit each for correlation using linear regression implemented by `LinMix`, including an intrinsic scatter and with uncertainties sampled by Markov Chain Monte Carlo (MCMC). In the case of logarithmic disk lag ratio, we treat the 27 lags with $\tau < 0$ as censored data in the `LinMix` fits by using their 1σ uncertainties as upper limits. The results of our linear fits against log(disk lag) ratio are provided in Table 1.

As a result of these linear fits, we identified two correlations with $>3\sigma$ significant trends between the tested quasar properties and disk lag ratio, and an additional correlation just shy of the 3σ level. None of our tested quasar properties correlated with our linear tested quantity disk lag offset, however. Figure 8 shows our observed anticorrelation between 3000 Å luminosity and log (disk lag) ratio. This correlation was also observed by Li et al. (2021) in a smaller sample of quasars. We also see an anticorrelation between X-ray luminosity and log(disk lag) ratio, implying that the disk lag offset may be related to the quasar's bolometric luminosity rather than monochromatic emission. The best-fit linear regression model of $\log(\tau_{\rm jav}/\tau_{\rm obs})$ versus 3000 Å and X-ray luminosity find slopes of $m = -0.38 \pm 0.10$, and $m = -0.36 \pm 0.15$, respectively. While the two trends are similar, the 3000 Å correlation is more significant ($>3\sigma$ inconsistent with zero). We see a similar correlation with black hole mass, with a slope of $m = -0.36 \pm 0.08$ (Figure 10).

Each of the anticorrelations found with the disk lag ratio exhibit similar slopes of $m \approx -1/3$. The functional form of SS73's predicted disk lag in Equation (3) shows $\tau_{\rm SS73} \propto L_{3000}^{1/3} M_{\rm BH}^{1/3}$. This $m \sim -1/3$ result would thus suggest that when L_{3000} and $M_{\rm BH}$ are fit independently, their anticorrelations are entirely dependent on their exponent in $\tau_{\rm SS73}$. This behavior is highlighted by the right panels of Figures 8, 9, and 10 where we show $\tau_{\rm jav}$ as a function of $\tau_{\rm SS73}$ for our 95 quasars. Luminosity and black hole mass do not exhibit any distinguishable behavior with respect to the $\tau_{\rm jav}$ axis.

While black hole mass and luminosity are connected through the Eddington ratio, possibly explaining the similarity in our found anticorrelations, our diverse sample quasar spans $10^{-3} < \lambda_{\rm Edd} < 10^{-0.5}$. To test better whether the black hole mass and luminosity anticorrelations are independent, we used a Bayesian maximum likelihood approach to multilinear regression to fit both simultaneously again the disk lag ratio. When using this approach, we rejected all measurements with $\tau_{\rm jav} < 0$, as the treatment of censored data was not implemented. The multilinear regression found similar slopes of $m = -0.22 \pm 0.09$ for luminosity and $m = -0.22 \pm 0.08$ for black hole mass, and exhibit excess scatter of $\sigma_{\rm excess} = 0.42$. In this case, the multilinear regression did not favor a single correlation for black hole mass or luminosity, and thus we conclude that these anticorrelations are likely independent. The shallower slopes of our multilinear regression may indicate that $\tau_{\rm jav}$ is not completely independent of luminosity and black hole mass, just not as influential as $\tau_{\rm SS73}$ predicts.

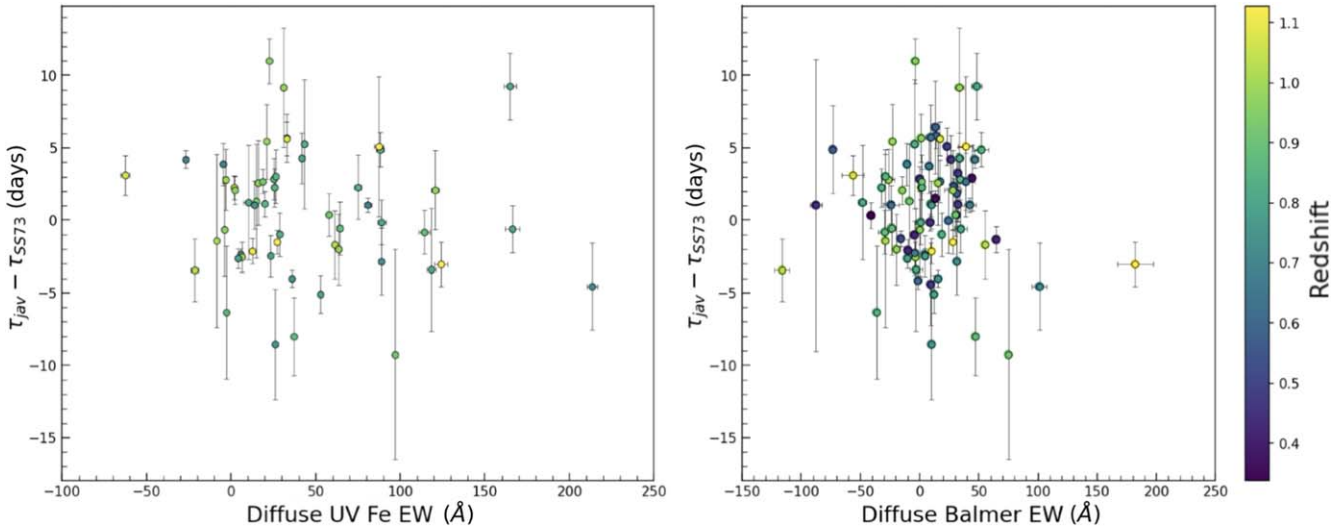

Figure 6. The measured rest-frame EWs of the Fe II (2250–2650 Å; left) and Balmer continua (3500–4000 Å; right) in the rms spectra, plotted against disk lag offset ($\tau_{jav} - \tau_{SS73}$) and colored by redshift. The points represent the mean of the distribution of EWs measured via the Monte Carlo method described in Section 3.2, while the error bars represent the standard deviation. There are 55 quasars with diffuse Fe II measurements, and 84 quasars with diffuse Balmer EW measurements, due to limited coverage of their respective regions in our rms spectra based on redshift. When fitting using `LinMix` as a Bayesian approach to linear regression, there was no correlation between disk lag offset and either of these diffuse EW measurements.

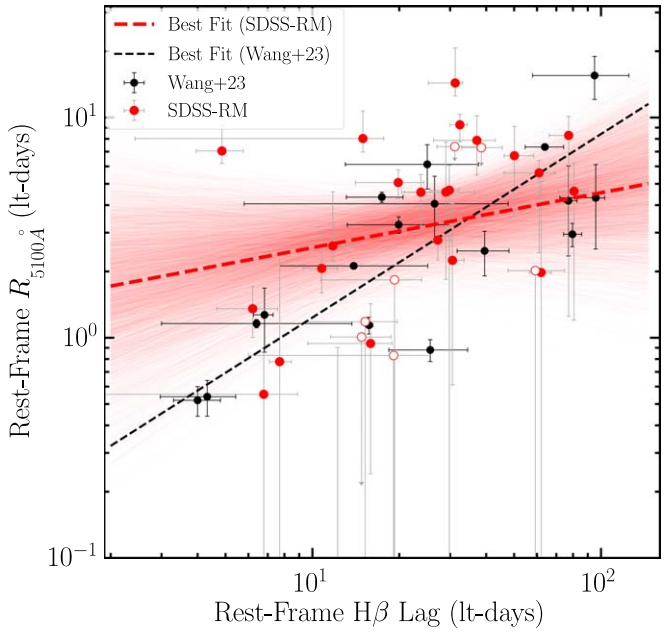

Figure 7. Comparison between the rest-frame 5100 Å continuum and Hβ lags for the SDSS-RM quasars (red) and AGNs studied by Wang et al. (2023; black). The black dashed line shows the best-fit relation of Wang et al. (2023). We perform a linear regression on the SDSS-RM measurements, including a survival analysis of seven lags with upper limits, with the red dashed line indicating the best-fit line and the collection of faint red lines showing the posteriors from the MCMC chain. The best-fit line for the SDSS-RM sample has a slope, formally consistent with zero, and $\sigma = 0.26$ excess scatter. We do not find a significant correlation between the continuum and BLR lags, further indicating that the continuum lags of the SDSS-RM quasars are not dominated by diffuse BLR emission.

Table 1
Quasar Properties that were Fit when Plotted against $\log(\tau_{jav}/\tau_{SS73})$ and the Slope of the Correlation and Excess Scatter of the Fit Including Uncertainties Found Using `LinMix`

Quasar Property	m	$\sigma_{scatter}$
λL_{3000}	$\mathbf{-0.38 \pm 0.10}$	0.40 ± 0.05
L_X (0.5–2 keV)	-0.36 ± 0.15	0.46 ± 0.06
M_{BH}	$\mathbf{-0.36 \pm 0.08}$	0.38 ± 0.05
λ_{EDD}	-0.02 ± 0.12	0.47 ± 0.06
Fe EW	-0.05 ± 0.03	0.47 ± 0.06
Fe/Hβ EW	0.07 ± 0.26	0.47 ± 0.06
Hβ EW	-0.02 ± 0.19	0.48 ± 0.06
$L_{O\,III}/L_{H\beta}$	0.01 ± 0.11	0.50 ± 0.07
He II EW	0.06 ± 0.05	0.47 ± 0.06

Note. Significant correlations with $m > 3\sigma$ are listed in bold.

4. Discussion

4.1. Diffuse BLR Contamination

In Section 3.2, we tested for the possibility of diffuse BLR emission contaminating the quasar light curves from the Balmer jump in the *i* band, and the "pseudocontinuum" of blended Fe II lines in the *g* band. These particular diffuse emission regions would affect quasars in the redshift range around $0.8 < z < 1.0$, where our AD test was inconclusive in determining whether these quasars were drawn from a different population of disk lag offsets compared to the whole sample of 95 quasars, shown in Figure 3. Further investigating the contribution of the Balmer jump and Fe II "pseudocontinuum," our measurements of their rms flux EWs show no correlation with disk lag offset.

Our results exploring diffuse emission differ from those for lower-luminosity local Seyfert 1 AGNs, in cases such as NGC 5548 (Fausnaugh et al. 2016; Cackett et al. 2022) and NGC 4593 (Cackett et al. 2018) where definitive excess lags in the ~3650 Å Balmer jump regime were found. Such significant diffuse BLR contamination may be more common for these lower-luminosity quasars due to the Baldwin (1977) effect, as referenced in Li et al. (2021) as a potential cause of the

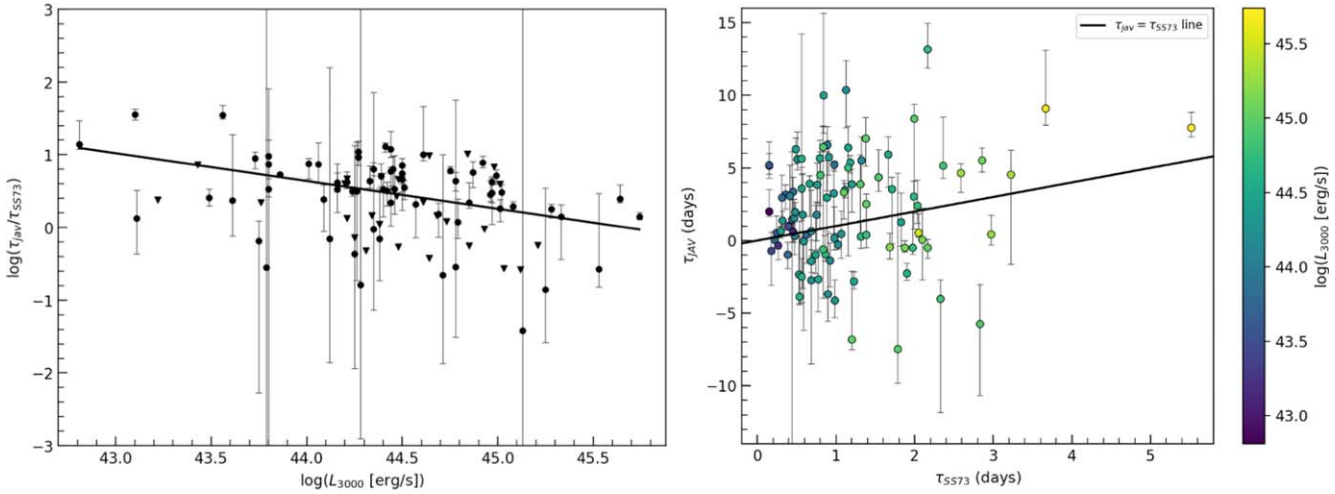

Figure 8. The relationship between disk lag and luminosity at 3000 Å (L_{3000}). The left plot shows an anticorrelation between the log-scaled disk lag ratio ($\log(\tau_{\rm jav}/\tau_{\rm SS73})$) and $\log(L_{3000})$ using the quasars from Homayouni et al. (2019), similar to the findings of Li et al. (2021) for their quasar sample. The black triangles with no error bars represent upper limits for the quasars that were measured to have $\tau_{\rm jav} < 0$. The resulting fit gives a slope of $m = -0.38 \pm 0.10$, an intercept of $b = 18 \pm 0.04$, and intrinsic scatter of $\sigma_{\rm scatter} = 0.40 \pm 0.05$. On the right is the measured lag using JAVELIN vs. the expected lag from the SS73 model, color-coded by $\log(L_{3000})$. The black line represents where the observed and model lags would be equal to help interpretation.

anticorrelation between disk lag ratio and luminosity, as we similarly show in Figure 8. The Baldwin effect is a well-known empirical anticorrelation between broad-line strength and luminosity for AGNs, which will be further discussed in Section 4.2. Our sample, with lags measured between the *g* and *i* bands corresponding to different rest-frame lags at different redshifts, should see an increased scatter in disk lag offset due to diffuse contamination affecting either the *g* or *i* band. Similar to the behavior of disk lag offset and redshift shown in Figure 2, the scatter in disk lag offsets is less for lower luminosities. If we are only considering diffuse Balmer contamination, which for the sample of quasars $z < 0.3$ and $L_{3000\ \text{Å}} < 10^{44}$ erg s^{-1} would contaminate the *g* band, we would expect shorter lags, counterintuitive to the anticorrelation found in Figure 8. Our sample shows little evidence of the Baldwin effect increasing diffuse BLR contamination, though expanding the comparison to a broader range of luminosity may probe the Baldwin effect better.

In addition to diffuse BLR emission features, continuum lags can potentially be influenced by more continuous optical emission from the BLR. BLR continuum light may be emitted in the form of reflected light from the accretion disk's continuum emission. The photoionization modeling performed in Korista & Goad (2001) suggests this effect should be relatively small, as the effective albedo of broad-line clouds is predicted to be much weaker than diffuse Balmer emission. More recent studies have begun to suggest additional emission across the full UV–optical range may originate from the BLR. Chelouche et al. (2019) and Cackett et al. (2022) find that lags need to be described by a combination of disk lags corresponding to the standard accretion disk and the BLR, in which continuous emission from the latter may originate from high-density material uplifted from the outer accretion disk. Contributions from BLR continuum emission would increase the measured lag but cannot explain the large scatter of lags both larger and smaller than predicted by the SS73 model found in our 95 quasar sample.

Starkey et al. (2023) address the accretion-disk size problem by introducing a steep rim to the edge of the accretion disk, as well as potential rippled structures throughout, all irradiated by the AGN's central lamppost. A rim in the outer accretion disk leads to longer lags in a similar way to diffuse BLR continuum emission, while highly irradiated ripples could satisfy the shorter-than-expected disk lags found within our sample.

We also tested our quasar sample for an $R_{\rm BLR}$–$R_{5100\ \text{Å}}$ correlation, which Wang et al. (2023) find to draw a connection to an $R_{5100\ \text{Å}}$–L relation. We do not find a significant correlation between the rest-frame continuum lag at 5100 Å and the rest-frame Hβ lag. Similar to our other results, this suggests that the continuum lags of SDSS-RM quasars are not dominated by diffuse BLR emission. There may be a tight $R_{5100\ \text{Å}}$–L relation for lower-luminosity Seyfert 1 AGNs, as found by Wang et al. (2023), but there is not a good correlation for the luminous quasars in the SDSS-RM sample.

4.2. Anticorrelations of Disk Lag Ratio with Luminosity and Black Hole Mass

As discussed in Section 3.3, numerous quasar properties were tested for correlations in the context of a linearly scaled disk lag offset, and log-scaled disk lag ratio. We did not find any significant relations against the linearly scaled disk lag offset, and no correlations with accretion rate, probed through various quantities related to eigenvector 1. The anticorrelations found were between the log-scaled disk lag ratios versus optical and X-ray luminosities, as well as black hole masses. These anticorrelations provide interesting implications regarding the accretion-disk size problem. Our multilinear regression fit between disk lag ratios, 3000 Å luminosities, and black hole masses found that neither correlation was dominant over the other.

In each case, these anticorrelations indicate larger disk lags for fainter and lower-mass quasars, with more agreement with the SS73 model predictions for more luminous and more massive quasars. Our results thus favor models that have increased continuum lags for fainter and lower-mass AGNs. One possibility for longer lags in less luminous quasars proposed in Li et al. (2021) is the Baldwin (1977) effect, if diffuse BLR emission contributes significantly to the continuum lags. While Baldwin (1977) originally found an anticorrelation between EW and luminosity predominantly in C IV, Lyα, and

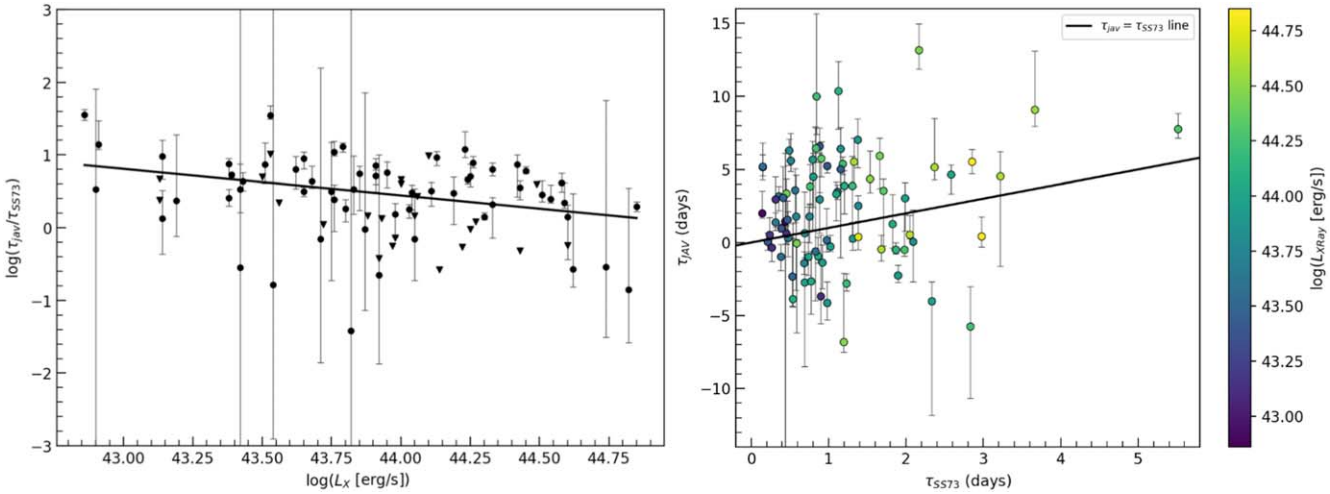

Figure 9. The relationship between disk lag and X-ray Luminosity (L_X) for 82 of the 95 quasars from Homayouni et al. (2019) that have measured L_X from Liu et al. (2020). The left plot shows an anticorrelation between the log-scaled disk lag ratio ($\log(\tau_{jav}/\tau_{SS73})$) and $\log(L_X)$, similar to the findings of Li et al. (2021) for their quasar sample. The black triangles with no error bars represent the upper limits for quasars that were measured to have $\tau_{jav} < 0$. The resulting fit gives a slope of $m = -0.36 \pm 0.15$, an intercept of $b = 16 \pm 6$, and intrinsic scatter of $\sigma_{scatter} = 0.46 \pm 0.06$. On the right is the measured lag using JAVELIN vs. the expected lag from the SS73 model, colored by $\log(L_X)$. The black line represents where the observed and model lags would be equal to help interpretation.

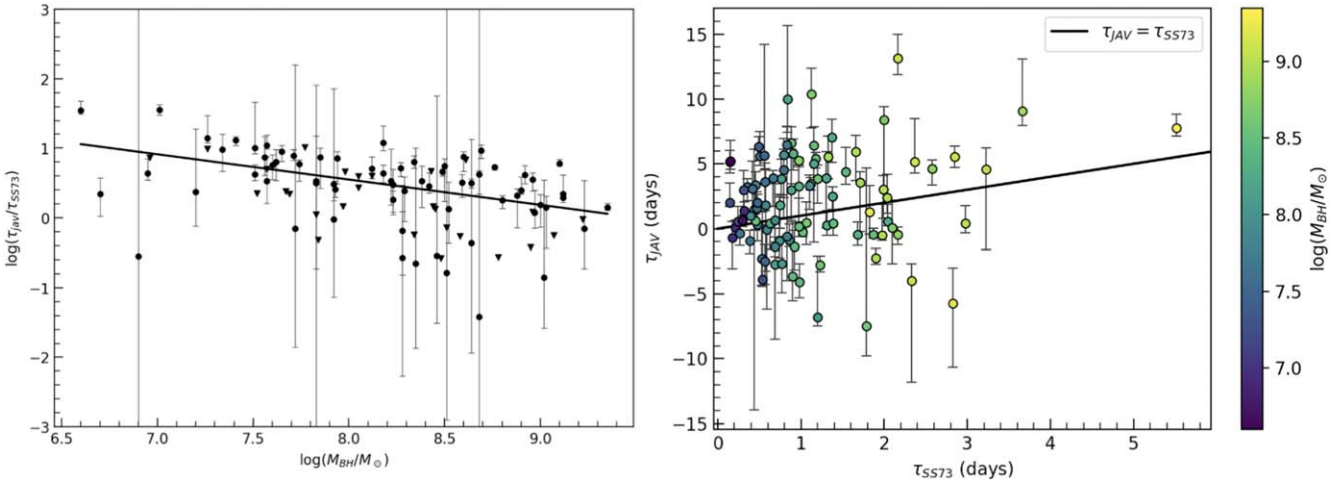

Figure 10. The relationship between disk lag and M_{BH}. The black triangles with no error bars represent upper limits to the quasar disk lag ratios that were measured to have $\tau_{jav} < 0$. The resulting fit gives a slope of $m = -0.36 \pm 0.08$, an intercept of $b = 3.5 \pm 0.7$, and intrinsic scatter of $\sigma_{scatter} = 0.38 \pm 0.05$.

C [III], other lines have been shown to have an EW dependence on luminosity, with higher-ionization lines exhibiting the steepest anticorrelations (Espey & Andreadis 1999; Dietrich et al. 2002). However, as discussed in Section 4.1, for our lower-luminosity and low-redshift quasars, diffuse BLR contamination poses the most bias from the Balmer jump in the g band, which would result in decreased lags with respect to the i-band light curves. Diffuse contamination and the Baldwin effect hence should not cause the observed excess lag at lower luminosities found within our quasar sample, as displayed in Figure 8. The Baldwin effect is not well studied in the context of diffuse BLR contamination, and can display shallow slopes for various lines ($EW \propto L^{-0.1}$; e.g., Espey & Andreadis 1999). Hβ EWs have even been shown to exhibit a slightly positive correlation with luminosity ($EW \propto L^{0.1}$; e.g., Netzer & Trakhtenbrot 2007), exhibiting an inverse Baldwin effect. As such, Li et al. (2021) stress the need for detailed BLR calculations to test this hypothesis properly. Our sample also shows no evidence for widespread diffuse BLR contamination of the continuum lags based on rms flux EWs, as discussed in Section 4.1. That said, our measurements are limited by a single g–i lag that probes different rest-frame continua at different redshifts, and our quasar sample includes quasars of different luminosities at different redshifts. More thoroughly testing for the potential influence of the Baldwin effect on diffuse BLR contamination requires multiband continuum RM of quasars spanning a broad range of luminosities.

Another plausible explanation for our observed anticorrelations, also discussed in Li et al. (2021), can be provided by the CHAR model (Sun et al. 2020), which considers magneto-hydrodynamic heating from a magnetically coupled corona and accretion disk. Such a mechanism would make the observed disk lag dependent on the thermal timescale, which for a steady-state disk occurs as $\tau_{TH} \propto L^{0.5}$. In this case, the thermal timescale has the largest deviation from the light-crossing time when quasars are less luminous, which would match the anticorrelation shown in Figure 8. The observed anticorrelation with black hole mass may have a similar explanation, with

smaller disks around smaller black holes showing a more noticeable contribution from τ_{TH} on top of the light-crossing time.

Kammoun et al. (2019) and Kammoun et al. (2021) additionally argue that changing the scale height of the X-ray corona can influence the measured continuum lag. Kammoun et al. (2021) predict a positive correlation between measured disk lag and X-ray luminosity, in contrast to our marginal anticorrelation between disk lag and X-ray luminosity. That said, our observed anticorrelation is marginal ($<3\sigma$), so definitive conclusions are harder to draw from the fit. Additionally, Kammoun et al. (2019) put heavy emphasis on the treatment of ionization in the disk along with corona height. We tested for correlations with L[O III]/L(Hβ) and He II EWs as proxies for ionization hardness but did not find any significant correlations. The lack of observed correlations may be because these quantities are poor proxies for the ionization driven by the central corona and/or because the connection between the corona and the reverberating disk is more complex than can be measured from simple quantities like L_X.

5. Summary

Using the 95 quasars from Homayouni et al. (2019), we explored how the distribution of disk lag measurements relate to their wide and diverse span of quasar properties across the sample. The results of fitting these quasar properties against the ratio of τ_{obs}/τ_{SS73} are summarized in Table 1. We additionally tested for the possibility of contamination by diffuse BLR emission in the measured continuum lags. The results of this work are as follows:

1. Luminosity and black hole mass are anticorrelated with disk lag ratio, as shown in Figures 8, 9, and 10. The 3000 Å luminosity and black hole mass anticorrelation exhibit a $>3\sigma$ significance, while the X-ray anticorrelation falls just under 3σ, each with slopes $\sim -1/3$. We found no correlation between disk lag ratio with other tested quasar properties associated with "eigenvector 1" and ionization hardness.
2. We find no evidence that the continuum lags have widespread contamination from diffuse BLR emission. There is no correlation between the presence of diffuse Fe II and Balmer emission in the rms spectra with differences in disk lags, and the disk lag offset distributions are consistent for quasars both in and outside the redshift range for which these diffuse BLR features fall in the observed filters. In contrast to Wang et al. (2023), we do not find a significant correlation between disk lag and BLR lag.

Our results in exploring diffuse contamination and the behavior of various quasar properties with the measured disk lag deviation from the SS73 model predictions appear to favor the CHAR model (Sun et al. 2020). For our sample, the effects of diffuse BLR contribution to the g- and i-band photometry has the potential for shorter and longer than expected lags, respectively, dependent on the redshift of a given quasar. Our quasar sample reproduces the luminosity anticorrelation with disk lag ratio found in Li et al. (2021), despite the lower-luminosity (lower redshift) quasars being more susceptible to diffuse Balmer contamination in the g band. Diffuse BLR contamination in the bluest light curve would result in smaller-than-expected lags, and as such, the Baldwin effect is a less favorable explanation of this anticorrelation.

Lags measured from a single pair of filters have limited ability to probe the wavelength-dependent contribution of diffuse BLR emission, even for a quasar sample spanning a broad range of redshifts. Given diffuse BLR emission has been proven to contribute to continuum light curves and influence lag measurements in low-redshift Seyfert 1 AGNs, future multiband continuum-RM surveys will better determine whether lower-luminosity quasars are more prone to diffuse BLR contamination via the Baldwin effect. In addition, frequency-resolved lags have the ability to probe roughly the reprocessing of particular emitting wavelengths on different timescales. This technique will prove useful in probing BLR photometric contributions and perhaps ripples in the accretion disk for the highest signal-to-noise ratio continuum-RM studies.

Acknowledgments

H.W.S., J.R.T., M.C.D., and L.B.F. acknowledge support from NSF grant CAREER-1945546, and with C.J.G. acknowledge support from NSF grants AST-2009539 and AST-2108668. C.R. acknowledges support from Fondecyt Regular grant 1230345 and ANID BASAL project FB210003. M.L.M.-A. acknowledges financial support from Millenium Nucleus NCN19-058 (TITANs).

Funding for SDSS-III was provided by the Alfred P. Sloan Foundation, the Participating Institutions, the National Science Foundation, and the U.S. Department of Energy Office of Science. The SDSS-III website is http://www.sdss3.org/. SDSS-III was managed by the Astrophysical Research Consortium for the Participating Institutions of the SDSS-III Collaboration including the University of Arizona, the Brazilian Participation Group, Brookhaven National Laboratory, Carnegie Mellon University, University of Florida, the French Participation Group, the German Participation Group, Harvard University, the Instituto de Astrofisica de Canarias, the Michigan State/Notre Dame/JINA Participation Group, Johns Hopkins University, Lawrence Berkeley National Laboratory, Max Planck Institute for Astrophysics, Max Planck Institute for Extraterrestrial Physics, New Mexico State University, New York University, Ohio State University, Pennsylvania State University, University of Portsmouth, Princeton University, the Spanish Participation Group, University of Tokyo, University of Utah, Vanderbilt University, University of Virginia, University of Washington, and Yale University.

Funding for the Sloan Digital Sky Survey IV has been provided by the Alfred P. Sloan Foundation, the U.S. Department of Energy Office of Science, and the Participating Institutions.

SDSS-IV acknowledges support and resources from the Center for High Performance Computing at the University of Utah. The SDSS website is www.sdss4.org.

SDSS-IV is managed by the Astrophysical Research Consortium for the Participating Institutions of the SDSS Collaboration including the Brazilian Participation Group, the Carnegie Institution for Science, Carnegie Mellon University, Center for Astrophysics—Harvard & Smithsonian, the Chilean Participation Group, the French Participation Group, Instituto de Astrofísica de Canarias, The Johns Hopkins University, Kavli Institute for the Physics and Mathematics of the Universe (IPMU)/University of Tokyo, the Korean Participation Group, Lawrence Berkeley National Laboratory, Leibniz Institut für

Astrophysik Potsdam (AIP), Max-Planck-Institut für Astronomie (MPIA Heidelberg), Max-Planck-Institut für Astrophysik (MPA Garching), Max-Planck-Institut für Extraterrestrische Physik (MPE), National Astronomical Observatories of China, New Mexico State University, New York University, University of Notre Dame, Observatário Nacional/MCTI, The Ohio State University, Pennsylvania State University, Shanghai Astronomical Observatory, United Kingdom Participation Group, Universidad Nacional Autónoma de México, University of Arizona, University of Colorado Boulder, University of Oxford, University of Portsmouth, University of Utah, University of Virginia, University of Washington, University of Wisconsin, Vanderbilt University, and Yale University.

We thank the Bok and CFHT Canadian, Chinese, and French TACs for their support. This research uses data obtained through the Telescope Access Program (TAP), which is funded by the National Astronomical Observatories, Chinese Academy of Sciences, and the Special Fund for Astronomy from the Ministry of Finance in China. This work uses observations obtained with MegaPrime/MegaCam, a joint project of CFHT and CEA/DAPNIA, at the Canada–France–Hawaii Telescope (CFHT), which is operated by the National Research Council (NRC) of Canada, the Institut National des Sciences de l'Univers of the Centre National de la Recherche Scientifique of France, and the University of Hawaii. The authors recognize the cultural importance of the summit of Maunakea to a broad cross section of the Native Hawaiian community. The astronomical community is most fortunate to have the opportunity to conduct observations from this mountain.

ORCID iDs

Hugh W. Sharp https://orcid.org/0000-0001-9616-1789
Y. Homayouni https://orcid.org/0000-0002-0957-7151
Jonathan R. Trump https://orcid.org/0000-0002-1410-0470
Scott F. Anderson https://orcid.org/0000-0002-6404-9562
Roberto J. Assef https://orcid.org/0000-0002-9508-3667
W. N. Brandt https://orcid.org/0000-0002-0167-2453
Megan C. Davis https://orcid.org/0000-0001-9776-9227
Logan B. Fries https://orcid.org/0000-0001-8032-2971
Catherine J. Grier https://orcid.org/0000-0001-9920-6057
Patrick B. Hall https://orcid.org/0000-0002-1763-5825
Keith Horne https://orcid.org/0000-0003-1728-0304
Anton M. Koekemoer https://orcid.org/0000-0002-6610-2048
Mary Loli Martínez-Aldama https://orcid.org/0000-0002-7843-7689
David M. Menezes https://orcid.org/0000-0003-4010-5336
Theodore Pena https://orcid.org/0000-0002-0033-5041
C. Ricci https://orcid.org/0000-0001-5231-2645
Donald P. Schneider https://orcid.org/0000-0001-7240-7449
Yue Shen https://orcid.org/0000-0003-1659-7035
Benny Trakhtenbrot https://orcid.org/0000-0002-3683-7297

References

Baldwin, J. A. 1977, ApJ, 214, 679
Blandford, R. D., & McKee, C. F. 1982, ApJ, 255, 419
Boroson, T. A., & Green, R. F. 1992, ApJS, 80, 109
Cackett, E. M., Bentz, M. C., & Kara, E. 2021, iSci, 24, 102557
Cackett, E. M., Chiang, C.-Y., McHardy, I., et al. 2018, ApJ, 857, 53
Cackett, E. M., Horne, K., & Winkler, H. 2007, MNRAS, 380, 669
Cackett, E. M., Zoghbi, A., & Ulrich, O. 2022, ApJ, 925, 29
Chelouche, D., Pozo Nuñez, F., & Kaspi, S. 2019, NatAs, 3, 251
Collier, S. J., Horne, K., Kaspi, S., et al. 1998, ApJ, 500, 162
Dalla Bontà, E., Peterson, B. M., Bentz, M. C., et al. 2020, ApJ, 903, 112
Dawson, K. S., Schlegel, D. J., Ahn, C. P., et al. 2013, AJ, 145, 10
Dexter, J., & Agol, E. 2010, ApJL, 727, L24
Dietrich, M., Hamann, F., Shields, J. C., et al. 2002, ApJ, 581, 912
Di Matteo, T., Croft, R. A. C., Springel, V., & Hernquist, L. 2003, ApJ, 593, 56
Di Matteo, T., Springel, V., & Hernquist, L. 2005, Natur, 433, 604
Edelson, R., Gelbord, J., Cackett, E., et al. 2017, ApJ, 840, 41
Edelson, R., Gelbord, J., Cackett, E., et al. 2019, ApJ, 870, 123
Edelson, R., Gelbord, J. M., Horne, K., et al. 2015, ApJ, 806, 129
Espey, B., & Andreadis, S. 1999, in ASP Conf. Ser. 162, Quasars and Cosmology, ed. G. Ferland & J. Baldwin (San Francisco, CA: ASP), 351
Event Horizon Telescope Collaboration, Akiyama, K., Alberdi, A., et al. 2019, ApJL, 875, L1
Fausnaugh, M. M., Denney, K. D., Barth, A. J., et al. 2016, ApJ, 821, 56
Fukugita, M., Ichikawa, T., Gunn, J. E., et al. 1996, AJ, 111, 1748
Gaskell, C. M. 2017, MNRAS, 467, 226
Gaskell, C. M., & Peterson, B. M. 1987, ApJS, 65, 1
Gaskell, C. M., & Sparke, L. S. 1986, ApJ, 305, 175
Gravity Collaboration, Sturm, E., Dexter, J., et al. 2018, Natur, 563, 657
Grier, C. J., Trump, J. R., Shen, Y., et al. 2017, ApJ, 851, 21
Hall, P. B., Sarrouh, G. T., & Horne, K. 2018, ApJ, 854, 93
Hernández Santisteban, J. V., Edelson, R., Horne, K., et al. 2020, MNRAS, 498, 5399
Homayouni, Y., Trump, J. R., Grier, C. J., et al. 2019, ApJ, 880, 126
Hopkins, P. F., Hernquist, L., Cox, T. J., et al. 2005a, ApJ, 630, 705
Hopkins, P. F., Hernquist, L., Cox, T. J., et al. 2005b, ApJ, 630, 716
Jiang, Y.-F., Green, P. J., Greene, J. E., et al. 2017, ApJ, 836, 186
Kammoun, E. S., Dovčiak, M., Papadakis, I. E., Caballero-García, M. D., & Karas, V. 2021, ApJ, 907, 20
Kammoun, E. S., Papadakis, I. E., & Dovčiak, M. 2019, ApJL, 879, L24
Kelly, B. C. 2007, ApJ, 665, 1489
Kelly, B. C., Bechtold, J., & Siemiginowska, A. 2009, ApJ, 698, 895
Kinemuchi, K., Hall, P. B., McGreer, I., et al. 2020, ApJS, 250, 10
Korista, K. T., & Goad, M. R. 2001, ApJ, 553, 695
Kormendy, J., & Ho, L. C. 2013, ARA&A, 51, 511
Kozłowski, S., Kochanek, C. S., Udalski, A., et al. 2010, ApJ, 708, 927
Li, T., Sun, M., Xu, X., et al. 2021, ApJL, 912, L29
Liu, T., Merloni, A., Simm, T., et al. 2020, ApJS, 250, 32
Lynden-Bell, D. 1969, Natur, 223, 690
MacLeod, C. L., Ivezić, Ž., Kochanek, C. S., et al. 2010, ApJ, 721, 1014
Magorrian, J., Tremaine, S., Richstone, D., et al. 1998, AJ, 115, 2285
Markoff, S. & Event Horizon Telescope Collaboration 2022, AAS Meeting Abstracts, 54, 211.01
McHardy, I. M., Cameron, D. T., Dwelly, T., et al. 2014, MNRAS, 444, 1469
McHardy, I. M., Connolly, S. D., Horne, K., et al. 2018, MNRAS, 480, 2881
Morgan, C. W., Kochanek, C. S., Morgan, N. D., & Falco, E. E. 2010, ApJ, 712, 1129
Mudd, D., Martini, P., Zu, Y., et al. 2018, ApJ, 862, 123
Mummery, A., & Balbus, S. A. 2020, MNRAS, 492, 5655
Netzer, H. 2022, MNRAS, 509, 2637
Netzer, H., & Trakhtenbrot, B. 2007, ApJ, 654, 754
Neustadt, J. M. M., & Kochanek, C. S. 2022, MNRAS, 513, 1046
Peterson, B. M., Ferrarese, L., Gilbert, K. M., et al. 2004, ApJ, 613, 682
Richards, G. T., Lacy, M., Storrie-Lombardi, L. J., et al. 2006, ApJS, 166, 470
Scholz, F. W., & Stephens, M. A. 1987, J. Am. Stat. Assoc., 82, 918
Sergeev, S. G., Doroshenko, V. T., Golubinskiy, Y. V., Merkulova, N. I., & Sergeeva, E. A. 2005, ApJ, 622, 129
Shakura, N. I., & Sunyaev, R. A. 1973, A&A, 500, 33
Shappee, B. J., Prieto, J. L., Grupe, D., et al. 2014, ApJ, 788, 48
Shen, Y., Brandt, W. N., Dawson, K. S., et al. 2015, ApJS, 216, 4
Shen, Y., Hall, P. B., Horne, K., et al. 2019, ApJS, 241, 34
Shen, Y., & Ho, L. C. 2014, Natur, 513, 210
Shen, Y., Horne, K., Grier, C. J., et al. 2016, ApJ, 818, 30
Soltan, A. 1982, MNRAS, 200, 115
Starkey, D. A., Horne, K., & Villforth, C. 2015, MNRAS, 456, 1960
Starkey, D. A., Huang, J., Horne, K., & Lin, D. N. C. 2023, MNRAS, 519, 2754
Sulentic, J. W., Calvani, M., & Marziani, P. 2001, Msngr, 104, 25
Sun, M., Xue, Y., Brandt, W. N., et al. 2020, ApJ, 891, 178
Tie, S. S., & Kochanek, C. S. 2018, MNRAS, 473, 80
Vestergaard, M., & Osmer, P. S. 2009, ApJ, 699, 800
Vincentelli, F. M., McHardy, I., Santisteban, J. V. H., et al. 2022, MNRAS: Lett., 512, L33
Virtanen, P., Gommers, R., Oliphant, T. E., et al. 2020, NatMe, 17, 261
Wang, S., Guo, H., & Woo, J.-H. 2023, ApJL, 948, L23
White, R. J., & Peterson, B. M. 1994, PASP, 106, 879
Yu, Z., Kochanek, C. S., Peterson, B. M., et al. 2020, MNRAS, 491, 6045
Yu, Z., Martini, P., Davis, T. M., et al. 2020, ApJS, 246, 16
Zu, Y., Kochanek, C. S., & Peterson, B. M. 2011, ApJ, 735, 80